

A possible global covariance between terrestrial gross primary production and ^{13}C discrimination: Consequences for the atmospheric ^{13}C budget and its response to ENSO

J. T. Randerson,¹ G. J. Collatz,² J. E. Fessenden,^{1,3} A. D. Munoz,¹ C. J. Still,⁴
J. A. Berry,⁵ I. Y. Fung,⁴ N. Suits,⁶ and A. S. Denning⁶

Received 2 December 2001; revised 21 August 2002; accepted 23 August 2002; published 20 December 2002.

[1] It is well known that terrestrial photosynthesis and ^{13}C discrimination vary in response to a number of environmental and biological factors such as atmospheric humidity and genotypic differences in stomatal regulation. Small changes in the global balance between diffusive conductances to CO_2 and photosynthesis in C3 vegetation have the potential to influence the ^{13}C budget of the atmosphere because these changes scale with the relatively large one-way gross primary production (GPP) flux. Over a period of days to years, this atmospheric isotopic forcing is damped by the return flux consisting mostly of respiration, Fire, and volatile organic carbon losses. Here we explore the magnitude of this class of isotopic disequilibria with an ecophysiological model (SiB2) and a double deconvolution inversion framework that includes time-varying discrimination for the period of 1981–1994. If the net land carbon sink and plant ^{13}C discrimination covary on interannual timescales at the global scale, consistent with El Niño-induced drought stress causing a decline in global GPP and C3 discrimination, then less interannual variability in ocean and land net carbon exchange is required to explain atmospheric trends in $\delta^{13}\text{C}$ and CO_2 as compared with previous studies that assumed discrimination was invariant. **INDEX TERMS:** 0322 Atmospheric Composition and Structure: Constituent sources and sinks; 1040 Geochemistry: Isotopic composition/chemistry; 1615 Global Change: Biogeochemical processes (4805); 1851 Hydrology: Plant ecology; **KEYWORDS:** global drought stress, tropical ecosystems, interannual variability of atmospheric $\delta^{13}\text{C}$, terrestrial carbon sinks, El Niño—Southern Oscillation

Citation: Randerson, J. T., G. J. Collatz, J. E. Fessenden, A. D. Munoz, C. J. Still, J. A. Berry, I. Y. Fung, N. Suits, and A. S. Denning, A possible global covariance between terrestrial gross primary production and ^{13}C discrimination: Consequences for the atmospheric ^{13}C budget and its response to ENSO, *Global Biogeochem. Cycles*, 16(4), 1136, doi:10.1029/2001GB001845, 2002.

1. Introduction

[2] El Niño-induced changes in ocean circulation and global climate affect atmospheric CO_2 concentrations through several different mechanisms. In the eastern Pacific, a shutdown in equatorial upwelling caused by a relaxation of trade winds leads to a decrease in mixed layer pCO_2

levels and in the ocean-to-atmosphere CO_2 flux [Feely *et al.*, 1997, 1999; Winguth *et al.*, 1994]. In terrestrial ecosystems, decreased strength of the Asian monsoon imposes widespread drought stress in southeast Asia and eastern Australia, the northern part of South America, Central America, and the Sahel in Africa [Dai *et al.*, 1997; Janicot *et al.*, 1996; Kripalani and Kulkarni, 1997]. Droughts in these regions are not fully compensated by wet spells in other regions: at the global scale precipitation decreases on land during El Niño events [Dai *et al.*, 1998]. The combination of drought stress and increased temperatures appears to increase carbon loss on land [Braswell *et al.*, 1997; Tian *et al.*, 1998; Potter and Klooster, 1999], although relative contribution of changes in gross primary production (GPP), ecosystem respiration, and fires is not well known.

[3] On El Niño—Southern Oscillation (ENSO) timescales (2–7 years), changes in atmospheric $\delta^{13}\text{C}$ (in conjunction with the growth rate of CO_2) have been used frequently as a diagnostic of interannual variability in ocean and land carbon fluxes [Ciais *et al.*, 1995; Enting *et al.*, 1995; Francey *et al.*, 1995; Keeling *et al.*, 1995; Battle *et al.*, 2000]. Known as a

¹Divisions of Geological and Planetary Sciences and Engineering and Applied Science, California Institute of Technology, Pasadena, California, USA.

²Goddard Space Flight Center, Greenbelt, Maryland, USA.

³Now at Hydrology, Geochemistry and Geology Group, Earth and Environmental Sciences Division, Los Alamos National Laboratory, Los Alamos, New Mexico, USA.

⁴Center for Atmospheric Sciences, University of California Berkeley, Berkeley, California, USA.

⁵Carnegie Institution of Washington, Department of Plant Biology, Stanford, California, USA.

⁶Department of Atmospheric Sciences, Colorado State University, Fort Collins, Colorado, USA.

“double deconvolution,” the $\delta^{13}\text{C}$ -derived record of terrestrial net carbon exchange has served as target (standard) for terrestrial ecosystem models attempting to reproduce inter-annual and decadal flux variability [Maisongrande et al., 1995; Thompson et al., 1996; Gerard et al., 1999; Potter and Klooster, 1999]. Previous applications of the double deconvolution approach have assumed that plant discrimination against ¹³C during photosynthesis remains constant from year-to-year. This approximation has been widely employed on many timescales [Joos and Bruno, 1998; Trudinger et al., 1999; Battle et al., 2000]. However, the potential of time varying discrimination to induce isotopic disequilibria has been recognized for several years [Lloyd and Farquhar, 1994; Francey et al., 1995; Ciais et al., 1995; Flanagan et al., 1997]. Studies of environmental and biological controls on ¹³C discrimination during photosynthesis have revealed a number of factors that cause discrimination to vary [Farquhar et al., 1989]. These include atmospheric humidity, solar radiation, drought stress, and plant type, all of which may be expected to respond to interannual climate variability.

[4] With the assumption of constant discrimination, the governing equations describing the atmospheric ¹³C budget simplify so that discrimination affects only the net land flux term and not the gross photosynthetic flux (GPP) term. Here we assess evidence that the global terrestrial biosphere, as a whole, experiences drought-stress during El Niño events. We also summarize theoretical and empirical evidence that drought-stress leads to predictable responses for GPP and ¹³C discrimination in C3 plants. We then provide a general framework for assessing the magnitude of isotopic disequilibria induced by time varying terrestrial ¹³C discrimination. We show that isotopic budgets for land need to include discrimination anomalies (much less than 1‰) interacting with the one-way total photosynthetic flux (which at the global scale has been estimated between 100–150 Pg C/yr). We suggest that a significant fraction of the accelerated decline in atmosphere $\delta^{13}\text{C}$ during latter stages of El Niño events may be attributed to a global decline in discrimination in tropical C3 ecosystems. Allowing discrimination to covary with GPP, in a double deconvolution inversion (presented below) suggests that land/ocean interannual flux variability may be substantially smaller than that predicted in previous analyses.

2. Methods

2.1. Climate Variability and Global Ecosystem Function

[5] To assess interannual changes in drought-stress at the global scale, we generated a monthly time series of precipitation (PPT), surface air temperature, and vapor pressure deficit (VPD) that were weighted spatially by net primary production (NPP) fluxes from the terrestrial biosphere. The rationale for this weighting function followed from our interest in the global budget of atmospheric ¹³C: anomalies in climate over land may have greater impact on the atmospheric budget when they occur in places with high plant productivity.

[6] We used the Global Precipitation Climatology Project Version 2 monthly product for PPT [Huffman et al., 1997; Susskind et al., 1997], the Goddard Institute for Space

Studies data set for surface air temperature [Hansen and Lebedeff, 1987; Hansen et al., 1999], and NCEP reanalysis products of 2-m relative humidity and air temperature for our VPD estimates [Kistler et al., 2001]. For the VPD estimates, we used surface air temperature as a proxy for internal leaf temperatures and monthly mean temperature and humidity data from NCEP (hence the relatively low estimates of VPD presented here). For the NPP-weighting function, we used the Carnegie-Ames-Stanford Approach (CASA) terrestrial biosphere model [Randerson et al., 1997]. NPP in CASA is derived from satellite-derived estimates of absorbed photosynthetically active radiation (PAR) [Bishop and Rossow, 1991; Los et al., 1994] and a light use efficiency term (units of g C/MJ PAR) that has a partial dependence on local environmental conditions. We used normalized estimates of the Southern Oscillation Index from the Australian Bureau of Meteorology (www.bom.gov.au/climate/current/soihtml.shtml).

[7] We constructed the NPP-weighted time series of climate variables (PPT, temperature, or VPD; denoted generically by W) using the following equation:

$$W(t) = \frac{\sum_x^{\text{land}} \sum_{i=1}^{12 \text{ months}} P(x, i) \cdot C(x, i, t)}{\sum_x^{\text{land}} \sum_{i=1}^{12 \text{ months}} P(x, i)} \quad (1)$$

where $P(x, i)$ represents the climatological mean NPP value for each grid cell, x , and month, i , and $C(x, i, t)$ represents the climate variable (PPT, temperature, or VPD) at each x , i , and year, t . We analyzed the 1980 to 2000 period, which included four El Niño events (1982–1983, 1987, 1991–1992, and 1997–1998), and two major volcanic eruptions (1982 and 1991) [Hansen et al., 1999].

2.2. Environmental and Physiological Controls on ¹³C Discrimination

[8] Variability in ¹³C discrimination, Δ_{ab} , by photosynthesis results from variability in discrimination along the pathway of CO₂ flux from the atmosphere through surface boundary layer, the stomatal pore, the cellular milieu and ultimately from fixation by rubisco, the primary carboxylation enzyme in photosynthesis.

$$C_a \xrightleftharpoons{g_b} C_s \xrightleftharpoons{g_s} C_i \xrightleftharpoons{g_m} C_c \xrightarrow{\text{Rubisco}}$$

$$\Delta_{\text{ab}} = b \frac{C_a - C_s}{C_a} + s \frac{C_s - C_i}{C_a} + m \frac{C_i - C_c}{C_a} + e \frac{C_c}{C_a} \quad (2)$$

where g_b , g_s and g_m are the conductances to CO₂ transport in the leaf boundary layer, stomatal pores and the cellular liquid phase (in the mesophyll) respectively. C_a , C_s , C_i and C_c are the CO₂ mole fraction in the atmosphere, leaf surface, intercellular spaces and chloroplasts respectively. b , s , m , and e represent discrimination factors associated with each step in the pathway (see Farquhar et al. [1989] for values). Rubisco discriminates strongly against ¹³CO₂ but overall discrimination is modulated by the ¹³CO₂ levels within the chloroplasts

that in turn are influenced by discrimination by diffusion along the gas and liquid phase pathways leading to the chloroplasts. C4 plants exhibit lower ¹³C discrimination because rubisco is isolated from diffusive interaction with the atmosphere as a result of the CO₂ concentrating mechanism found in these plants which discriminates relatively little [Farquhar *et al.*, 1989].

[9] Studies of leaves and plants reveal that though discrimination capacity of rubisco is relatively constant among species, the ¹³C/¹²C ratio of CO₂ in the chloroplasts may vary in response to environmental conditions and species characteristics causing overall discrimination to vary. Perhaps the most well studied and significant source of variability in C3 plants occurs from the diffusion of CO₂ through the stomata [Berry, 1987]. Lower stomatal conductances cause the intercellular CO₂ concentration during steady state photosynthesis to fall and the ¹³C/¹²C ratio of that CO₂ to increase relative to the outside atmosphere. Stomatal conductance is strongly coupled to photosynthesis (i.e., rubisco activity) in a way that tends to maintain intercellular CO₂ concentrations (and thus the internal ¹³C/¹²C) at fairly constant levels [Wong *et al.*, 1979]. However, as the vapor pressure gradient between the leaf and the atmosphere increases, stomatal conductance declines relative to photosynthetic capacity reducing intercellular CO₂, increasing the ¹³C/¹²C of internal CO₂, countering discrimination by rubisco and lowering overall discrimination by photosynthesis. An equation developed by Farquhar *et al.* [1982] provides a quantitative basis for predicting these changes in discrimination as a function of intercellular CO₂. Other evidence suggests that water stress and high solar radiation levels can also lead to lower overall discrimination [Farquhar *et al.*, 1989]. There is also a tendency for herbaceous species to discriminate more than woody species as a result of interspecific differences in stomatal conductance relative to photosynthetic capacity [Ehleringer, 1993].

[10] To illustrate and quantify how environmental and physiological conditions affect discrimination, we used the SiB2 land surface model that includes photosynthesis and stomatal conductance parameterizations [Sellers *et al.*, 1996b] allowing diagnosis of component and overall discrimination during photosynthesis at hourly time steps. The previously described version of SiB2 has been updated to include a diffusive conductance for CO₂ between the intercellular spaces and the sites of rubisco catalyzed carboxylation. This conductance is in series with CO₂ diffusion across the leaf boundary layer and the stomata (N.S. Suits *et al.*, Simulating seasonal and spatial variations in global concentrations and carbon isotopic ratios of atmospheric CO₂, in preparation for *Global Biogeochemical Cycles*, 2002). The value of mesophyll conductance, g_m , is a function of the maximum capacity for photosynthesis (rubisco activity or V_{max} [see Evans and Loreto, 2000]), a water availability scaling factor, $w(\theta)$ that depends on water filled pore space in the soil, and the canopy integration factor, Π [Sellers *et al.*, 1996b]. The canopy integration factor, Π , scales the mesophyll conductance for a leaf at the top of the canopy to a bulk canopy value analogous to the approach used to calculate canopy photosynthesis and stomatal conductance [Sellers *et al.*, 1996a]. Here n is a

scaling parameter tuned so that $C_i - C_c$ was about 50 ppm mole fraction for light saturated unstressed photosynthesis.

$$g_m = n \cdot V_{max} \cdot \Pi \cdot w(\theta) \quad (3)$$

In SiB2 stomatal conductance is represented by

$$g_c = m_{bb} \frac{A_c}{C_s} h_s + b_c \quad (4)$$

where h_s and b_c are canopy bulk leaf surface humidity and minimum conductance respectively. m_{bb} is an empirical constant that can be viewed as the reciprocal of the intrinsic water use efficiency (and in the definition of terms given here it also includes the diffusion coefficient of CO₂ relative to water vapor). The smaller the value of m_{bb} the higher the water use efficiency, the lower C_i/C_a and the lower Δ_{ab} becomes. Canopy photosynthesis, A_c , is a function of C_c , short wave solar radiation, temperature, and soil water availability (and V_{max}). In SiB2 A_c is equivalent to GPP minus leaf respiration.

[11] We used meteorological conditions [Sellers *et al.*, 1989] and vegetation parameters [Sellers *et al.*, 1996a] from an Amazonian forest to test the sensitivity of discrimination to environmental conditions and model parameters. Sensitivities (S) are expressed as

$$S = \frac{\Delta V}{V} \frac{P}{\Delta P} \quad (5)$$

where V is the dependent variable [e.g., discrimination ($^{13}\Delta_{ab}$) or canopy photosynthesis (A_c)] and P is a parameter or independent variable. We also calculated the sensitivity of Δ_{ab} for a given change in A_c caused by a change in P . While not strictly a sensitivity estimate, it does reflect how discrimination and photosynthesis change relative to one another which is important for evaluating the influence of vegetation on atmospheric CO₂ and δ_a as will be shown below. Environmental conditions (atmospheric humidity, solar radiation) and model parameters ($FPAR$, V_{max} , intrinsic water use efficiency ($1/m_{bb}$), and n) were reduced individually by 20% for the calculation of respective S values. Water stress response was estimated by initializing model simulations at lower soil water content causing the water stress factor to increase by 14% and reducing A_c by about 10%. Model parameters ($FPAR$, V_{max} , m_{bb} , and g_m) can be considered as surrogates for physiological/biological controls on discrimination. Dependent variables were expressed as averages of hourly values weighted by A_c .

2.3. Implications for the Global Atmospheric ¹³C Budget

2.3.1. Conventional Double Deconvolution Approach

[12] The atmospheric mass balance of total C in CO₂ can be described by the following equation:

$$\frac{d(C_a)}{dt} = N_b + N_o + F_f \quad (6)$$

where the atmospheric rate of change $d(C_a)/dt$ is equal to fossil fuel (F_f) release and uptake by ocean (N_o) and land

Table 1. Description of Symbols Used in the Text, and Values Used to Construct Figure 5

Symbol	Value	Description
C_a	750 Pg C	mass of carbon in the atmosphere
F_f	6.0 Pg C/yr	annual global fossil fuel and cement flux
N_b		net carbon flux to C3 land plants
N_o		net carbon flux to the oceans
δ_a	-7.8‰	$\delta^{13}\text{C}$ composition of the atmosphere
$d(C_a)/dt$	3.0 Pg C/yr	rate of change of atmospheric carbon
$d(\delta_a)/dt$	-0.02‰/yr	rate of change of the $\delta^{13}\text{C}$ composition of the atmosphere
G_b	~ -125 Pg C/yr GPP $G_b' \sim -32$ Pg C/yr (Figure 5)	gross atmosphere-terrestrial biosphere flux (GPP) In Figure 5 we use G_b' instead of G_b for illustration purposes: We assume that all C3 plant respiration and 1/3 of heterotrophic respiration occurs during the same year as G_b , and so this component of the flux does not impact the annual ^{13}C or CO_2 budgets illustrated in Figure 5. Also, we only considered a change in the C3 component which accounts for $\sim 77\%$ of global NPP (section 2.3.3).
R_b	~ 125 Pg C/yr $R_b' \sim 31$ Pg C/yr (Figure 5)	gross terrestrial biosphere-atmosphere return flux. In Figure 5, we isolate the component of R_b that has a residence time in the biosphere that is longer than 1 year, denoted here by R_b' (section 2.3.3). R_b and R_b' include the Suess Effect.
δ_f	-28‰	$\delta^{13}\text{C}$ composition of fossil fuel emissions
$\bar{\Delta}_{ab}$	19‰	mean C3 ^{13}C plant discrimination. We assume in analysis of Figure 5 that the terrestrial sink is C3.
$\dot{\Delta}_{ab}$	$0.01 * \bar{\Delta}_{ab} = 0.19\%$	Changes in C4 productivity are discussed in section 4.3. anomaly in C3 ^{13}C discrimination. In Figure 5 we explore the implications of a discrimination anomaly that is 1% of the mean C3 value.
δ_{ba}	$\delta_{ba} - \bar{\Delta}_{ab} = -7.8\% - 19.0\%$	$\delta^{13}\text{C}$ composition of the terrestrial biosphere-atmosphere return flux in Figure 5 (red arrow).
$\bar{\epsilon}_{ao}$	-1.8‰	mean ^{13}C discrimination associated with net ocean uptake
G_o	90 Pg C/yr	gross ocean-atmosphere flux
$\delta_a^{eo} - \delta_a$	0.6‰	isotopic disequilibria of the ocean-atmosphere flux
$\delta_a^{eb} - \delta_a$	0.33‰	isotopic disequilibria of the terrestrial biosphere-atmosphere flux

(N_b) net carbon sinks. With equation 1, N_o and N_b are unknown and so an additional constraint (from O_2/N_2 ratios [Keeling et al., 1996] or ^{13}C [Tans et al., 1993]) is required to distinguish between the two sinks. For the case of ^{13}C , a second equation can be written in δ notation that captures the difference in isotopic fractionation associated with photosynthesis and air-sea gas exchange [Francey et al., 1995]:

$$\begin{aligned} \frac{d(\delta_a C_a)}{dt} &= \bar{\delta}_a \frac{d(C_a)}{dt} + \bar{C}_a \frac{d(\delta_a)}{dt} \\ &\cong N_b(\delta_a - \bar{\Delta}_{ab}) + G_b(\delta_a^{eb} - \delta_a) + \delta_f F_f + N_o(\bar{\epsilon}_{ao} + \delta_a) \\ &\quad + G_o(\delta_a^{eo} - \delta_a) \end{aligned} \quad (7)$$

where the rate of change in atmospheric ^{13}C is approximately equal to isotopic changes imposed by a terrestrial carbon sink, terrestrial disequilibria forcing (caused by the changing atmospheric isotope composition), fossil fuel isotope forcing, ocean uptake, and ocean disequilibria forcing (see Table 1 for a definition of the various terms in equations (6)–(9)).

[13] Using atmospheric measurements, along with characterization of fossil fuel $^{13}\text{C}/^{12}\text{C}$ composition, fractionation by photosynthesis and ocean exchange, and models of carbon

turnover in terrestrial and oceanic reservoirs, it is possible to solve these two equations to estimate terrestrial and ocean carbon sinks at various spatial and temporal scales.

2.3.2. Proposed Framework for Variable Plant Discrimination

[14] The representation of biosphere-atmosphere ^{13}C fluxes described by equation (7) includes an implicit assumption that discrimination against ^{13}C during photosynthesis is invariant. A more general description of biosphere-atmosphere exchange allows for the possibility of a changing discrimination:

$$\frac{d(C_a)}{dt} = G_b + R_b + N_o + F_f \quad (8)$$

$$\begin{aligned} \frac{d(\delta_a C_a)}{dt} &\cong G_b(\delta_a - \bar{\Delta}_{ab} - \dot{\Delta}_{ab}) + R_b(\delta_{ba}) + \delta_f F_f + N_o(\bar{\epsilon}_{ao} + \delta_a) \\ &\quad + G_o(\delta_a^{eo} - \delta_a) \end{aligned} \quad (9)$$

where the net land flux, N_b , is now replaced with the sum of GPP (G_b) and the biosphere-atmosphere return flux (R_b). While R_b is largely composed of plant and heterotrophic respiration (R_a and R_h), fire and volatile organic carbon losses are also included in this term. Discrimination is now defined as the sum of an invariant mean, $\bar{\Delta}_{ab}$, and a time

varying anomaly, Δ_{ab} . In Appendix A, we show that if Δ_{ab} is assumed to equal to 0, then equation (9) simplifies to equation (7). However, when Δ_{ab} is not equal to zero, the product $G_b\Delta_{ab}$ has the potential to induce an atmospheric forcing. This atmospheric forcing is erased as the isotopic composition of respiration (δ_{ba}) adjusts to (equilibrates with) the new value of discrimination.

[15] With equations (8) and (9), there are now five unknowns, Δ_{ab} , R_b , δ_{ba} , G_b , and N_o , and two constraints: the atmospheric rate of change of CO_2 and $\delta^{13}\text{CO}_2$. Three additional pieces of information are needed to solve this more general system of equations. They are described in the following three subsections.

2.3.2.1. Anomalies in Plant Discrimination

[16] Variability in Δ_{ab} arises from physiological, ecosystem, and biome-level factors. A model that couples stomatal conductance and photosynthesis may capture some of the response of internal leaf CO_2 concentrations and ^{13}C discrimination to short-term environmental variability at leaf and canopy levels. When environmental perturbations persist for a period of weeks to seasons, the integrated ecosystem response will also reflect changes in the contribution to the gross flux from species with different intrinsic growth rates, allocation patterns, and water use efficiencies. At the biome level, changes in the disturbance regime can affect the distribution of different plant functional types such as C3 trees and C4 grasses.

2.3.2.2. Magnitude of the Biosphere–Atmosphere Return Flux

[17] At a given time interval, it may be possible to estimate R_b from an ecosystem model that takes into account carbon accumulation (the past history of G_b), allocation, and if available, contemporary information on rates of decomposition, plant respiration, fire, and other loss pathways.

2.3.2.3. Isotopic Composition of the Biosphere–Atmosphere Return Flux

[18] Accurate estimates of δ_{ba} are challenging because they require integration of the past history of G_b , Δ_{ab} , Δ_{ab} , and δ_a , and information about biosphere-atmosphere loss pathways. For example, the carbon released by fire has a different isotopic composition than that released from the same ecosystem by decomposition because of differences in the chemical composition and ages of substrates consumed by the two processes [Schuur *et al.*, 2002].

2.3.3. Vector Diagram of ^{13}C and CO_2 Budgets for 1990

[19] To illustrate the difference between conventional (equations (6) and (7)) and general (equations (8) and (9)) descriptions of terrestrial biosphere isotopic exchange, we constructed a mean annual ^{13}C and CO_2 atmospheric budget for a single year (1990) using data from multiple sources [Andres *et al.*, 2000; Francey *et al.*, 1995; Fung *et al.*, 1997; Gruber and Keeling, 2000; Tans *et al.*, 1993] as summarized in Table 1. We present these budgets using the vector diagram approach developed by Enting *et al.* [1993]. For the conventional budget diagram, terrestrial fluxes were partitioned into net sink and disequilibrium components. For the general budget diagram, we estimated the component of the gross biosphere-atmosphere flux that would

retain a discrimination anomaly after 1 year. With both the general and conventional budgets, we considered the effect of a 1% change in global terrestrial C3 discrimination over a year (i.e., a global change from 19.0‰ to 19.19‰).

[20] We assumed that 77% of GPP is C3 [Still *et al.*, 2002], NPP is $\sim 50\%$ of GPP [Ryan, 1991; Woodwell and Whittaker, 1968], and that all plant respiration is respired in the same year as initial fixation so these fluxes have no impact on the annual atmospheric ^{13}C budget. Of the remaining C3 NPP, we assumed that $\sim 1/3$ was released via herbivory, microbial decay, and fire during the same year as the initial fixation (see paragraph below). The component of C3 NPP that remained in the ecosystem after 1 year was assumed to consist of carbon allocated to wood (with very long residence times), and the fraction of leaves and fine roots not consumed by herbivores, microbial decay, or fires. With these assumptions, and starting with a global GPP of 125 Pg C/yr, we obtained a C3 NPP flux of 32 Pg C/yr that retained our hypothetical 1% discrimination anomaly after 1 year. We denote this decimated flux as G'_b .

[21] A precise estimate of G'_b is difficult because it requires accurate assessments of plant allocation, longevity estimates of fine roots, leaves, and stems, decomposition rates of these plant tissues, and the distribution of plant functional types at regional and global scales. Compared with other biosphere models used in isotope studies, our estimate of G'_b is conservative (low). For example, with the five-box model of the biosphere constructed by Emanuel *et al.* [1981] and employed by Francey *et al.* [1995], approximately 70 Pg C (out of an original GPP flux of 120 Pg C/yr) remained in the biosphere after 1 year [Thompson and Randerson, 1999]. Similarly, with the CASA model approximately 45 Pg C (out of an original NPP flux of 55 Pg C/yr) remained in the biosphere after 1 year [Thompson and Randerson, 1999].

[22] A significant fraction of G'_b consists of NPP allocated to wood (that remains intact within plants typically for a period far in excess of 1 year). Using the CASA biosphere model as a tool to help with scaling, we found that between 7.8 Pg C/yr and 15.1 Pg C/yr of global NPP was allocated to wood, with the variation depending largely on whether a fixed biome vegetation map (upper estimate [DeFries and Townsend, 1994]) or a map of fractional woody vegetation cover (lower estimate [DeFries *et al.*, 2000]) was used with the model allocation scheme (G. van der Werf, personal communication, 2002).

[23] The physiological and ecosystem studies that provide the underpinnings for these models also provide direct evidence that our estimate of G'_b is conservative. Tropical dry forest trees, temperate (cold) deciduous trees, and perennial grasses store starches and sugars in stems and boles at the end of one growing season for the purpose of rapid canopy construction at the onset of the following growing season [Aerts and Chapin, 2000]. Thus, some small component of plant respired C (autotrophic respiration) has a residence time of a year or more. Of the remaining carbon that contributes to a cohort of NPP, rapid loss pathways are likely to be leaf and fine root decomposition, herbivory, and fire. For the case of litter decomposition losses to the atmosphere, the C residence time

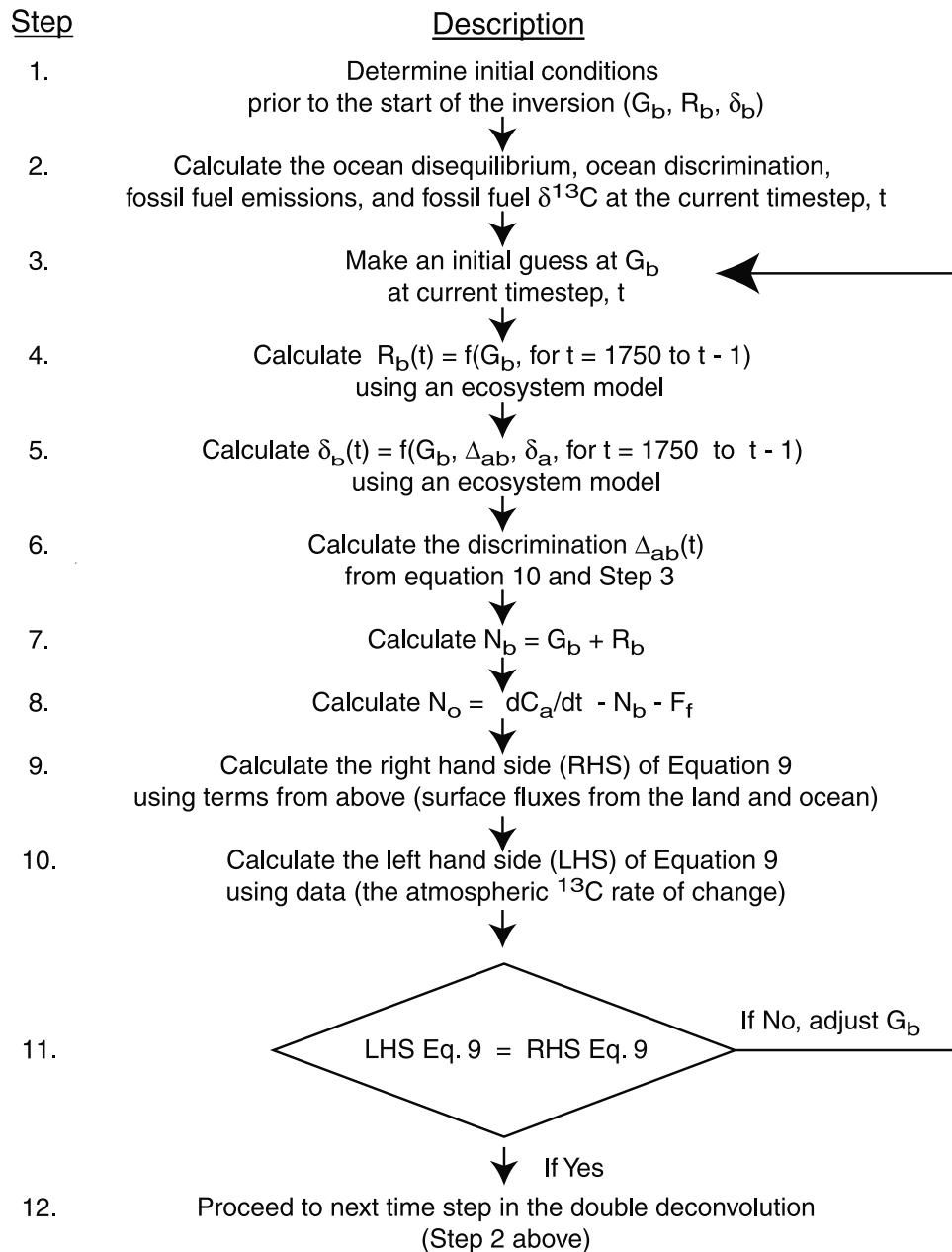


Figure 1. We solved a variable discrimination inversion with CO_2 and $\delta^{13}\text{C}$ using an iterative approach with equations (8), (9), and (10). The steps in the iteration are outlined with this flowchart. Prior to 1750, the atmosphere was assumed to be in steady state isotopically with the terrestrial biosphere (no disequilibria).

must also include the lifetime of leaves and fine roots. For tropical and boreal evergreen species, leaf lifespan typically varies between 1 and 2 years [Aerts and Chapin, 2000]. Even for deciduous trees, forbs, and grasses, the mean leaf lifespan is about 0.5 years [Aerts and Chapin, 2000]. Decomposition of leaf litter adds another 0.3 to 0.75 years to the biosphere residence time of carbon allocated to leaves in tropical ecosystems and from 1 to 10 years in temperate and boreal ecosystems [Aerts and Chapin, 2000]. Root longevity and rates of decomposition are more uncertain, and occur on a timescale of weeks to

years. A considerable fraction of fine roots appear to live for periods greater than 1 year in temperate forests [Gaudinski et al., 2000]. Finally, fires release no more than 5 Pg C/yr to the atmosphere [Crutzen and Andreae, 1990], and it is likely that a large component of fire emissions have a residence time in the terrestrial biosphere longer than 1 year.

2.3.4. A Simplified Double Deconvolution Inversion With Variable Discrimination

[24] We made two simplifications that allowed us to solve for the ^{13}C and total CO_2 budgets using equations (8) and

(9). First, if GPP and discriminations do covary at regional and global scales in response to drought stress, then it may be possible to write a linear equation relating discrimination anomalies to GPP anomalies:

$$\Delta_{ab} = S_A^\Delta \left(\frac{G_b - \bar{G}}{\bar{G}} \right) \cdot \bar{\Delta}_{ab} \quad (10)$$

where S_A^Δ is a linear scaling factor that describes how an annual anomaly in GPP translates into an anomaly in discrimination, i.e., a sensitivity factor. S_A^Δ will vary over the land surface depending on what environmental variables are regulating productivity and the timescales that are considered (see sections 2.2, 3.2, and 4.2). Where concurrent productivity and isotope data are (or become) available, direct measurement of S_A^Δ provides a means for testing the tropical and global scale discrimination-GPP covariance hypothesis presented here.

[25] In our preliminary analysis presented here, we used S_A^Δ values of 0.0 and 0.50 in an iterative double deconvolution process described below (Figure 1). A S_A^Δ value of 0.0 represents invariant discrimination, i.e., the conventional double deconvolution approach (equations (6) and (7)). A S_A^Δ value of 0.5 corresponds to the following: a 1% change in annual GPP causes a 0.5% change in annual (flux-weighted) discrimination. The 0.5 S_A^Δ value we adopted is conservatively consistent with the response of C3 tropical forest in SiB2 to the sum of VPD and soil moisture effects (sections 2.2, 3.2, and 4.2) and is broadly consistent with many (but not all) tree ring studies that measured both growth increments and wood isotopic composition (see section 4.2 for a more detailed discussion).

[26] The second simplification is that we used a 1-D pulse response (Green's function) model of the terrestrial biosphere with a monthly time step to estimate R_b as a function of the past history of GPP and δ_{ba} as a function of the past history of G_b , Δ_{ab} , $\bar{\Delta}_{ab}$, and δ_a . Our pulse model only considered the C3 terrestrial biosphere, and started with C3 GPP of $\sim 90 \text{ Pg C/yr}$ in 1750. From 1750 to 1981, ice core records of δ_a [Francey et al., 1999] were used as a boundary condition for the pulse model, to properly capture the isotopic disequilibria of the changing atmosphere (or Suess Effect). Similarly, we increased NPP from 1750 to 1982, following atmospheric CO_2 (with a β factor of 0.4 [Wullschlegel et al., 1995]), to generate a difference between G_b and R_b required by the double deconvolution approach at the start of the 1981–1994 period.

[27] With this simple pulse-response approximation, interannual variation in climate did not affect the magnitude of R_b , and we assumed that C4 ecosystems did not contribute to interannual variation in gross or net terrestrial exchange. These assumptions allow for a simplistic representation of the terrestrial biosphere, allow us to demonstrate the consequences of C3 discrimination variability for the global carbon budget, but are insufficient for a comprehensive assessment of changes in atmospheric $\delta^{13}\text{C}$ and CO_2 (see section 4.4).

[28] For this analysis, we used a smoothed atmospheric record of $\delta^{13}\text{C}$ and CO_2 record from Cape Grim archived air from 1982 to 1994 [Francey et al., 1999]. We solved

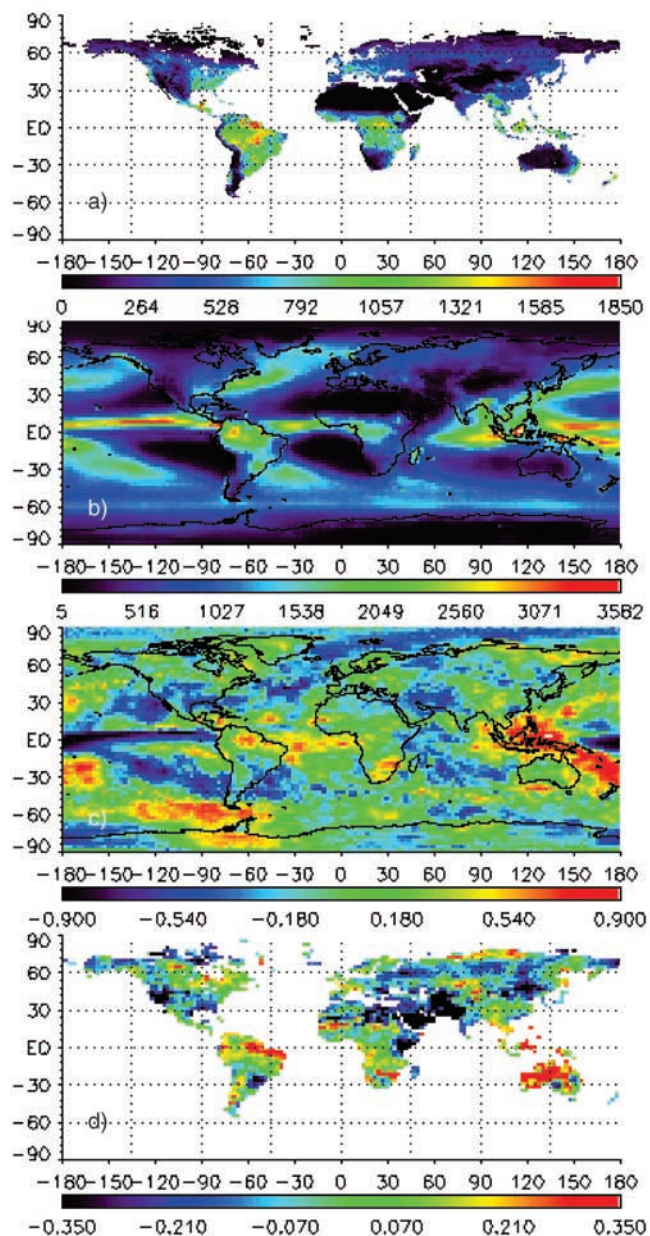


Figure 2. (a) Annual NPP from the CASA model is greatest in equatorial regions of South America, Africa, and Asia ($\text{g C m}^{-2} \text{ yr}^{-1}$). This NPP product is derived primarily from satellite-derived products of normalized difference vegetation index (NDVI) and solar radiation (see text for details). (b) Global precipitation (PPT) from the GPCP Version 2 monthly product (mm yr^{-1}) has a very similar global pattern to NPP. (c) Pearson correlation coefficient, r , between annual PPT and a normalized Southern Oscillation Index (SOI) (unitless) for the 1980–2000 period. In positive correlation areas (denoted by red), rainfall decreases during El Niño events. Note the relatively high correlation coefficients in northern South America, Southeast Asia, and western equatorial Africa, where both mean annual NPP and PPT are large. (d) The fractional difference in mean annual PPT between a La Niña period (1999 and 2000) and an El Niño period (1997 and 1998) (unitless).

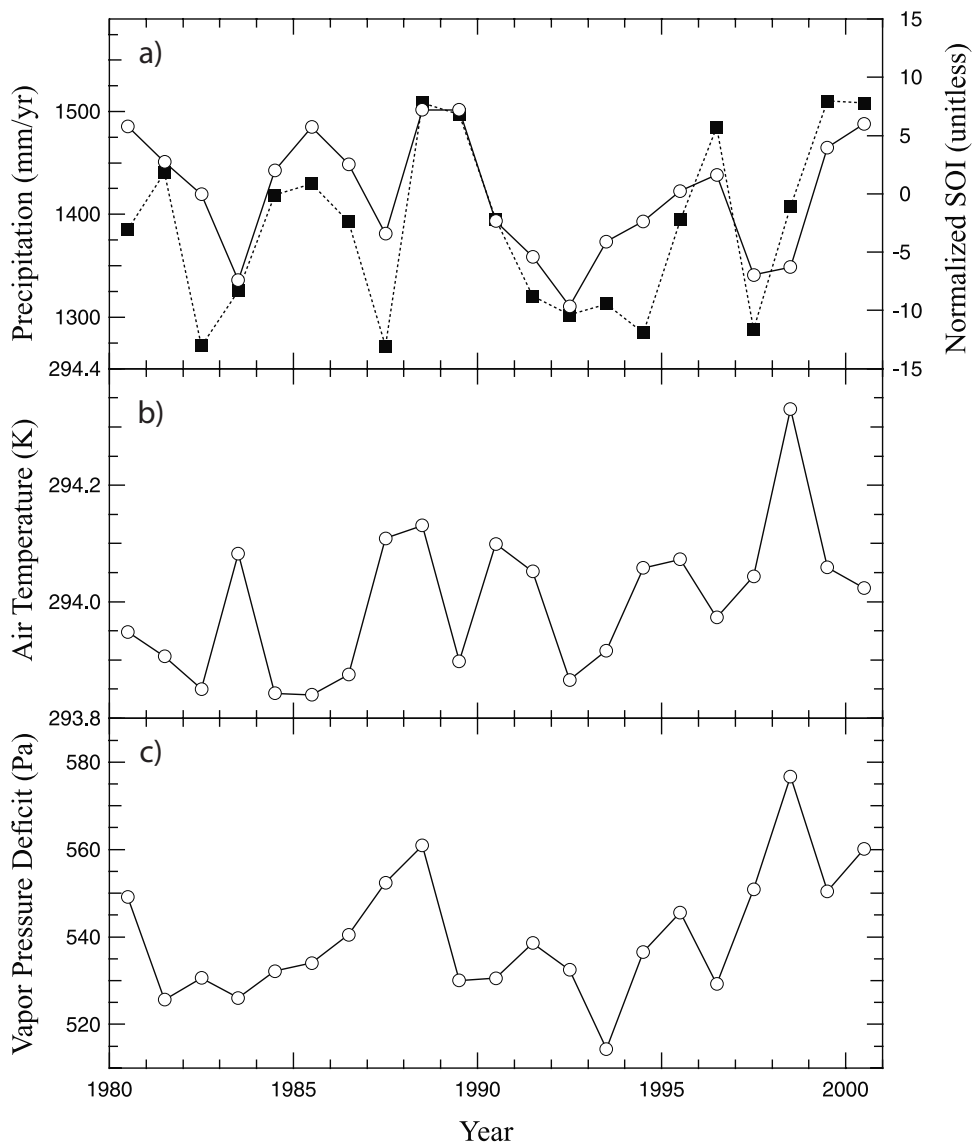


Figure 3. (a) NPP-weighted precipitation, (b) surface air temperature, and (c) vapor pressure deficit time series were calculated according to equation (1) (solid line with circles). The normalized Southern Oscillation Index (SOI) was highly correlated with rainfall over the terrestrial biosphere (dashed lines with squares) over the 1980 to 2000 period. NPP-weighted precipitation varied by over 13% during this period. The global terrestrial biosphere experienced drought stress during the 1982–1983, 1987, and 1997–1998 El Niño events, as measured by low rainfall, high air temperatures, and high vapor pressure deficits.

equations (8), (9), and (10) using an iterative process (Figure 1).

3. Results

3.1. Climate Variability and Global Ecosystem Function

[29] Mean annual NPP derived from satellite-derived estimates of canopy light absorption was highest in equatorial regions of South America, Africa, and Asia (Figure 2a) and had a similar spatial pattern to mean annual PPT (Figure 2b). Interannual PPT was strongly correlated with

the Southern Oscillation Index in northern South America, southern Africa, southeast Asia, and eastern and northern Australia (Figure 2c). Weak positive correlations occurred over western equatorial Africa and western boreal North America. Negative correlations occurred over the central part of North America, the southeastern part of South America, and central Asia. Decreases in PPT during the 1997–1998 El Niño event were substantial over many regions (in excess of 35%) when compared with PPT during the 1999 to 2000 La Niña period (Figure 2d).

[30] Over the entire terrestrial biosphere (equation (1)), PPT changed substantially from year-to-year, with a 13%

difference between the maximum rate in 1989 and the minimum rate in 1992 (Figure 3a). The relatively strong 1997–1998 El Niño event caused a global decrease in biosphere-weighted PPT of 5% in 1997 and in 1998, relative to the long-term mean. Biosphere-weighted PPT was also below average during other El Niño events of varying intensity: 1983, 1987, and 1991–1992. Biosphere-weighted PPT had a significant positive correlation with the Southern Oscillation Index from 1980 to 2000 ($r = 0.75$, $n = 19$, $P < 0.05$) (Figure 3a).

[31] Biosphere-weighted temperatures reached a maximum in 1998 during the 1997–1998 El Niño event. The lowest biosphere-weighted temperature during the 1980–2000 period occurred in 1992, probably as a result of stratospheric aerosol loading from the Pinatubo volcanic eruption in June of 1991 (Figure 3b). Biosphere-weighted VPD obtained from NCEP data varied by over 11% from 1980 to 2000. The maximum VPD (0.58 kPa) occurred in 1998, while the minimum VPD (0.51 kPa) occurred in 1993 (Figure 3c).

3.2. GPP and Discrimination Responses to Environment and Physiology

[32] The influences of atmospheric vapor pressure deficit (VPD) and $FPAR$ on Δ_{ab} and A_c are illustrated in Figure 4. A_c increased by more than $20 \mu\text{mol CO}_2 \text{ m}^{-2} \text{ s}^{-1}$ as a result of increasing $FPAR$ from 0.2 to 0.9 (a change in leaf area index from 0.5 to 5) causing Δ_{ab} to increase by about 0.7‰ to 1.1‰ depending on VPD. Positive feedback between A_c , g_c , and h_s caused C_i/C_a and Δ_{ab} to increase with $FPAR$. A 33% increase in VPD (from 16.4 hPa to 21.9 hPa) reduced Δ_{ab} by about 0.4‰ to 0.8‰ depending on A_c .

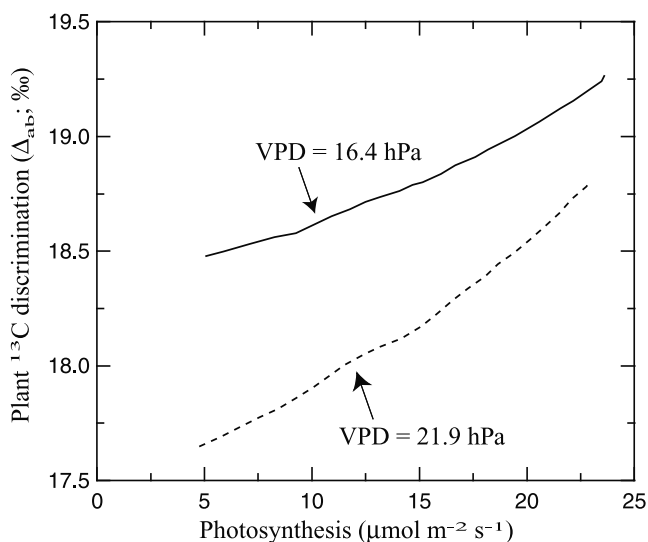


Figure 4. C3 discrimination from the SiB2 model is highly sensitive to VPD. Each model trajectory was created by varying canopy LAI between 0.5 and 5.0. The upper trajectory (solid line) was obtained by using meteorological conditions for a tropical forest site from *Sellers et al.* [1989]. The lower trajectory (dashed line) was created by increasing mean VPD by 33% relative to the meteorological conditions used in the upper trajectory.

Table 2. Sensitivity of Canopy Photosynthesis (GPP) and ^{13}C Discrimination to Climate and Model Parameters^a

Dependent Variable	Sensitivity of Δ_{ab}	Sensitivity of GPP	S_A^Δ (equation (10))
<i>Climate</i>			
VPD	-0.08	-0.10	0.79
PAR	-0.09	0.49	-0.18
soil water availability	0.12	0.68	0.24
<i>Model Parameter</i>			
FPAR	0.07	1.07	0.06
V_{max}	0.06	0.60	0.10
m_{bb}	0.29	0.52	0.56
n	0.15	0.21	0.70

^aVPD is the vapor pressure deficit of the atmosphere, PAR is the incident photosynthetically active radiation, FPAR is the fraction of PAR absorbed by the canopy, V_{max} is the maximum rubisco capacity, and n is the mesophyll conductance scalar.

[33] Table 2 shows the sensitivities (S) to environmental conditions likely to vary on interannual timescales, specifically, VPD, photosynthetically active radiation (PAR) and soil water availability. Increasing VPD causes stomata to close, decreasing C_i/C_a and C_c/C_a . Since both A_c and Δ_{ab} are functions of C_c there is a near proportional change in Δ_{ab} relative to A_c as VPD changes. Reducing water stress has a smaller effect because in our model parameterization water stress affects the flux A_c , and the conductances, g_c and g_m linearly which tends to maintain C_c constant. The fact that there is moderate sensitivity is in part a result of feedback between A_c , g_c , h_s and C_i . That is, water stress reduces A_c and g_c causing reduced transpiration and increased leaf temperatures. The resulting lower h_s reduces g_c further relative to A_c such that C_i and thus C_c and Δ_{ab} decrease. Increasing PAR increases A_c and g_c but does not influence g_m causing C_c and Δ_{ab} to decrease slightly.

[34] Model parameters reflect the characteristics of the vegetation. Specifically, $FPAR$ indicates the amount of green canopy, V_{max} the photosynthetic capacity of the leaves, m_{bb} the reciprocal of the intrinsic water use efficiency of the leaves and n , the mesophyll capacity for CO_2 transport. These characteristics vary among species and for an individual plant depending on environmental conditions. Though in SiB2 m_{bb} is constant for specific vegetation types, previous studies show that plants adapted or exposed to water stress conditions can have higher intrinsic water use efficiencies (lower m_{bb}) which would have the net effect of increasing Δ_{ab} relative to GPP [*Farquhar et al.*, 1989; *Ehleringer*, 1993]. $FPAR$ and V_{max} have only small impacts on S_A^Δ and n tends to be fairly conservative among various types of plants [*Evans and Loreto*, 2000]. The high sensitivity for changes in n does illustrate the potentially strong influence that the parameterization of g_m can have on predictions of S_A^Δ .

3.3. Implications for the Global Atmospheric ^{13}C Budget

3.3.1. Vector Diagram of ^{13}C and CO_2 Budgets for 1990

[35] Different amounts of discrimination against ^{13}C by C3 photosynthesis ($\sim 19\text{‰}$) and by air-sea gas exchange

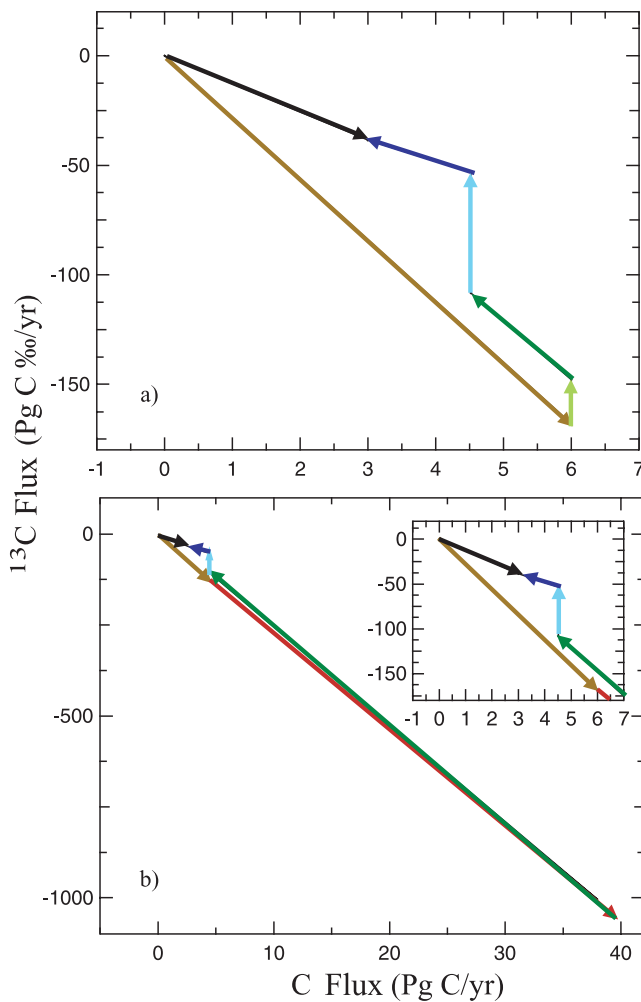


Figure 5. (a) Conventional double deconvolution inversion approach for estimating land and ocean carbon sinks for 1990. The brown vector represents fossil fuel emissions (6 Pg C/yr, -168 Pg C $\text{‰}/\text{yr}$), the light green vector represents the land isotopic disequilibrium forcing (0 Pg C/yr, 20 Pg C $\text{‰}/\text{yr}$), and the light blue represents the ocean disequilibrium forcing (0 Pg C/yr, -55 Pg C $\text{‰}/\text{yr}$). The black vector represents the observed change in atmospheric composition (3.0 Pg C/yr, -38 Pg C $\text{‰}/\text{yr}$). Only one combination of land (dark green vector) and ocean (dark blue vector) net carbon sinks can close both the ^{13}C and total C budgets. (b) The land flux can be alternately represented as the difference between the two one-way gross exchanges of GPP (G'_b , dark green vector) and the biosphere-atmosphere return flux (R'_b , red vector). Note the change in axis scale between Figures 5a and 5b. The land isotopic disequilibria forcing term (arising from the Suess effect) is the same in Figures 5a and 5b, but in Figure 5b it is included as a part of R'_b . The two approaches, Figures 5a and 5b, are equivalent when discrimination is invariant (Appendix A), but rapidly diverge when discrimination anomalies change the slope of G'_b .

($\sim 2\%$ as a global ocean average) uniquely determine the slope of the net land and ocean carbon sink vectors shown in Figure 5a. A 1% change in global ^{13}C discrimination (the slope of the dark green arrow) with the conventional double deconvolution representation (Figure 5a) will have a negligible impact on land/ocean sink partitioning: less than 0.02 Pg C/yr shift between land and ocean sinks.

[36] With the more general description of the terrestrial biosphere, a 1% change in annual C3 ^{13}C discrimination (0.19‰) has a substantial impact on the land/ocean sink partitioning: a 0.37 Pg C/yr shift between land and ocean sinks (equations (8) and (9)). This increased impact on land/ocean sink partitioning occurs because the discrimination anomaly changes the slope of the relatively large gross atmosphere-biosphere terrestrial flux vector (G'_b , note the change in scale between Figures 5a and 5b). We assumed that 2/3 of C3 NPP retained the 1% discrimination anomaly after 1 year (see section 2.3.1).

3.3.2. A Double Deconvolution Inversion With Variable Discrimination

[37] During the 1980s and early 1990s, smoothed trends in atmospheric CO_2 and $\delta^{13}\text{C}$ were highly variable (Figures 6a and 6b). For example, the El Niño event of 1982–1983 was characterized by large growth rates of atmospheric CO_2 and large decreases in $\delta^{13}\text{C}$. In contrast, during the early 1990s, CO_2 growth rates were smaller and $\delta^{13}\text{C}$ decreases almost ceased.

[38] In our inversion analysis, an almost neutral terrestrial biosphere in the early 1980s and a large terrestrial carbon sink in the early 1990s provided the best fit with atmospheric observations (Figure 6c). When discrimination was held constant, the terrestrial carbon sink ranged between -0.3 Pg C/yr and -2.7 Pg C/yr over the 13-year period. When discrimination was allowed to covary with GPP, the terrestrial carbon sink ranged between -0.4 Pg C/yr and -2.1 Pg C/yr. The effect of allowing discrimination to covary with GPP in our simplified inversion was to decrease the range of the terrestrial carbon sink by 0.7 Pg C/yr or 28%. The impact on the range of the ocean sink was more modest: a decrease in the range by 0.4 Pg C/yr or 14%. With the constant discrimination inversion, the mean difference between the ocean and land sink in any given year was 1.0 Pg C/yr, whereas with variable discrimination, the mean difference was 0.6 Pg C/yr (this represents over a 40% reduction).

[39] The range of GPP required to sustain a terrestrial carbon sink over this period (to keep photosynthesis outpacing respiration) was substantially less when discrimination was allowed to covary with GPP (Figure 6d). In the inversion with constant discrimination, C3 discrimination was fixed at 19‰. When GPP and discrimination were allowed to covary, discrimination of the C3 terrestrial biosphere ranged between 18.9‰ and 19.3‰ (Figure 6e). This range represents less than a 2% change in the discrimination of the C3 terrestrial biosphere.

4. Discussion

4.1. Climate Variability and Global Ecosystem Function

[40] The PPT, temperature, and VPD data presented in Figures 2 and 3 suggest that the terrestrial biosphere, as a

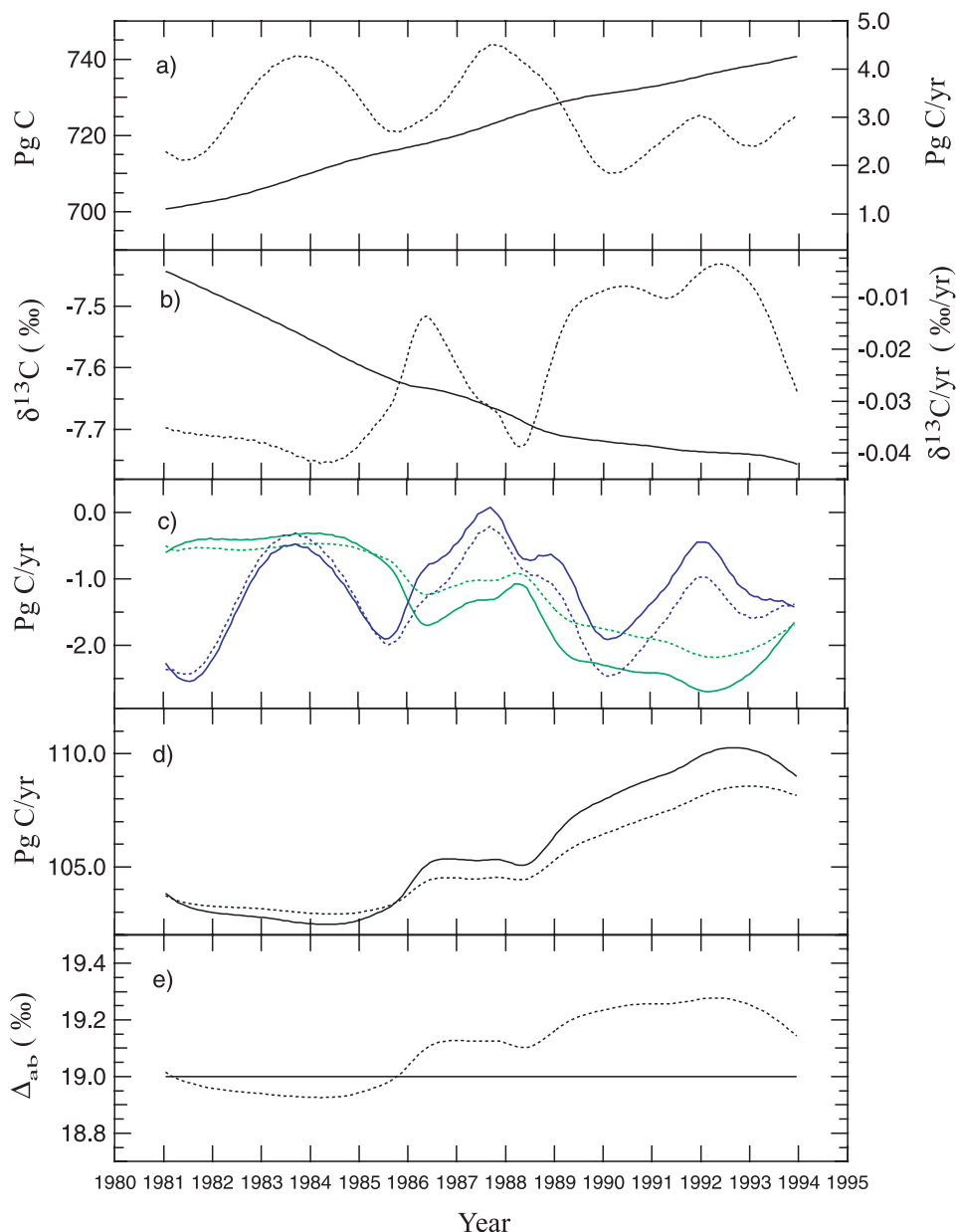


Figure 6. Driving data and results from a 1-dimensional double deconvolution inversion with variable discrimination. (a) The atmospheric CO_2 content (left axis) and its annual rate of change (right axis) [Francey *et al.*, 1999]. (b) The atmospheric $\delta^{13}\text{C}$ composition (left axis) and its annual rate of change (right axis) [Francey *et al.*, 1999]. (c) An inversion with constant discrimination (solid lines) and with variable discrimination that varies linearly with global GPP (dotted lines). Ocean fluxes are denoted by blue and terrestrial biosphere fluxes are denoted by green. (d) Changes in GPP required to sustain a terrestrial carbon sink for the constant (solid) and variable discrimination (dotted) inversion cases. Plant respiration and decomposition were calculated using a pulse-response model of the terrestrial biosphere [Thompson and Randerson, 1999]. (e) Discrimination for the constant (solid) and variable (dotted) inversion cases.

whole, undergoes drought stress during major El Niño events like the one in 1997–1998. Biosphere-weighted PPT decreased, while biosphere-weighted temperature increased (Figure 3). Anomalously high air temperatures enhanced atmospheric driving gradients for water loss. The

primary regions of the terrestrial biosphere that experienced below normal rainfall levels were Central America, northern South America, southern Africa, Southeast Asia, and northern and eastern Australia. These areas account for a substantial fraction of global terrestrial NPP (Figure 2a). Other

analyses of PPT using station data from the last century suggest that the magnitude of PPT decreases in these regions is substantial during El Niño events [Dai et al., 1997; Janicot et al., 1996; Kripalani and Kulkarni, 1997; Ropelewski and Halpert, 1996] and that when PPT anomalies are integrated over all land areas, the signal remains strong [Dai et al., 1998]. Ropelewski and Halpert [1996] found that for large areas of central America, northeastern South America, India, southeastern Asia, and Australia, PPT decreased by about 20% to 40% during El Niño warm events relative to the long-term mean, and by twice that amount relative to the mean of La Niña cold events. Satellite observations during the last two decades confirm that leaf area (or FPAR) decreased during major El Niño events in these regions (and globally) and that terrestrial vegetation growth is linked with interannual patterns of sea surface temperature and PPT [Asner et al., 2000; Kogan, 2000; Los et al., 2001].

[41] Together, this climate and satellite evidence suggests that at the global scale, ENSO-induced change in water availability is the single most important factor that regulates interannual fluxes from the terrestrial biosphere. During the 1982–1983, 1987, and 1997–1998 El Niño events, the growth rate of atmospheric CO_2 significantly increased in the mid to latter stages of the event [Conway et al., 2001], although a quantitative partitioning of mechanisms remains elusive [Yang and Wang, 2000]. The terrestrial biosphere component of the anomalies probably involved some combination of decreased GPP [Tian et al., 1998], enhanced respiration [Braswell et al., 1997], and greater fire losses [Nepstad et al., 1999].

4.2. Environmental and Physiological Controls on ^{13}C Discrimination

[42] The SiB2 model simulations illustrate the short time-scale physiological responses to drought that determine GPP and Δ_{ab} in tropical C3 vegetation. Changes in Δ_{ab} relative to A_c (or GPP) are particularly significant in response to VPD, soil water availability, and intrinsic water use efficiency. Large-scale drought conditions brought on by an El Niño would include soil water stress, higher VPD and higher PAR all of which would tend to decrease Δ_{ab} . In addition, increases in water use efficiency brought on by plant response to drought or by a reduction in herbaceous plant productivity (a shift toward woody species) can lead to lower Δ_{ab} . At the ecosystem scale, plants with lower C_i/C_a may do proportionally better than plants with higher C_i/C_a in response to drought; i.e. drought stress over a period of months to years may amplify flux contributions from plants with higher water use efficiencies and lower discrimination values. The combination of these factors is likely to cause GPP and Δ_{ab} to covary at interannual timescales.

[43] Interannual changes in precipitation water availability associated with ENSO can impose large changes in stand-level GPP and canopy conductance [Goldstein et al., 2000]. What is more difficult to predict is the response of ecosystem respiration relative to GPP, given that increasing temperatures will increase metabolic activity of plants and microbes [Ryan, 1991; Lloyd and Taylor, 1994], but decreased water availability will decrease growth respiration

and the flow of dissolved organic compounds through the soil, a flux that is required for microbial metabolism [Neff and Asner, 2001; Raich and Potter, 1995]. In a temperate deciduous forest, decreases in respiration following a drought outpaced the decline in photosynthesis, leading to net CO_2 uptake by the ecosystem [Goulden et al., 1996]. Although interannual ecosystem flux data from tropical ecosystems is relatively sparse, evidence of deep taproots and access to deep soil water reserves in seasonally dry forests [Nepstad et al., 1994] suggests that in the tropics, ecosystem respiration may also be more sensitive to drought stress as compared with GPP.

[44] While the impacts of El Niño on ecosystem respiration are ambiguous, it is clear that one of the primary impacts of ENSO-induced drought stress in tropical forests is to increase fire frequency and intensity. Global estimates of biomass burning are between 2 and 4.5 Pg C/yr, and largely occur in seasonally dry tropical forests and savannas [Crutzen and Andreae, 1990]. While interannual variability in biomass burning is not well quantified, aircraft trace gas measurements (and in particular $\text{CO}:\text{CO}_2$ ratios) provide evidence that anomalously high levels of biomass burning occurred during the 1997–1998 El Niño [Matsueda and Inoue, 1999]. Other impacts of El Niño in tropical forests include increased tree mortality [Villalba and Veblen, 1998] and forest impoverishment [Nepstad et al., 1999].

[45] Experimental evidence at the ecosystem scale for a covariance between GPP and discrimination in ecosystems that undergo drought stress comes from several sources. Saplings grown under low levels of water availability exhibit decreased instantaneous photosynthesis rates and water use efficiencies, long-term plant growth, and plant discrimination [Ares and Fownes, 1999; Zhang et al., 1997]. Measurement of phloem $\delta^{13}\text{C}$ increased by as much 8‰ from the wet to dry season in Australian eucalyptus forests, whereas irrigation fed stands exhibited almost no seasonal response and had an annual mean value that was depleted by over 3‰ as compared with the nonirrigated stands [Pate and Arthur, 1998]. Many tree ring studies report a negative correlation between tree ring growth increments (a surrogate for productivity) and wood isotopic composition in regions that undergo interannual variability in drought [Barber et al., 2000; Livingston and Spittlehouse, 1993; McNulty and Swank, 1995; Saurer et al., 1995]. It is important to note, however, not all tree ring analyses show a significant negative relations between growth indices and isotope composition [Flanagan et al., 1997; Stuiver et al., 1984], and in the tropics, where drought-stress is likely to be a major driver of productivity changes, there are few published interannual time series of productivity and plant ^{13}C discrimination from tree rings or other sources.

[46] Other isotopic work at the ecosystem scale suggests that the effects of water availability on discrimination are substantial and immediate. Over the course of a growing season in temperate forest ecosystems, the isotopic composition of soil respiration closely tracks water availability and can vary by up to 4 or 5‰ [Bowling et al., 2002; Ekblad and Hogberg, 2001; J. E. Fessenden and J. Ehleringer, Temporal variation in $\delta^{13}\text{C}$ of ecosystem respiration in the

Pacific Northwest: Links to moisture stress, submitted to *Oecologia*, 2002]. *Bowling et al.* [2002] provide evidence that the link between humidity and the isotopic composition of soil respiration occurs rapidly (with a lag only of a few days) implying rapid changes in ecosystem water use efficiency and rapid C turnover within the soil.

4.3. Implications for the Global Atmospheric ^{13}C Budget

[47] If GPP and discrimination covary at regional and global scales, then less interannual variability in net land and ocean carbon fluxes may be needed to explain atmospheric $\delta^{13}\text{C}$ anomalies. During the later stages of the 1982–1983 and 1997–1998 El Niño events, the rate of decline in atmospheric ^{13}C accelerated [*Battle et al.*, 2000; *Francey et al.*, 1995]. Our analysis suggests that part of this acceleration may be simply a result of some combination of vegetation VPD response and increased water use efficiency and thus lower than average discrimination in tropical C3 ecosystems. A negative anomaly in discrimination would provide less resistance to the dilution of atmospheric $\delta^{13}\text{C}$ by fossil fuels, independent of any changes in the net terrestrial flux.

[48] A negative anomaly in discrimination, while accelerating the decline in atmospheric $\delta^{13}\text{C}$ during the initial El Niño event, may have the opposite effect on the atmosphere in subsequent years because of feedbacks through the terrestrial biosphere. Although these feedbacks may not have been fully captured with our simple pulse-response biosphere model, they would work in the following way. Organic matter that was fixed during the initial drought stress event will be relatively enriched in $\delta^{13}\text{C}$. As this carbon is released back to the atmosphere in subsequent years, it will tend to enrich the atmosphere as compared with respiration of an average isotopic composition.

[49] The initial response of global discrimination to El Niño along with feedbacks in subsequent years, have the combined effect in double deconvolution analyses of requiring less interannual variability in the net land carbon sink to account for atmospheric anomalies $\delta^{13}\text{C}$. Because ocean and land carbon sinks are solved for simultaneously in equations (8), (9), and (10), ocean sink variability also decreases when terrestrial discrimination is allowed to vary with GPP. Thus, the mechanism described here may help to reconcile differences between the double deconvolution approach and other (less variable) methods used to estimate ocean fluxes [*Lee et al.*, 1998].

[50] While changes in atmospheric O_2/N_2 levels are consistent with large year-to-year changes in the terrestrial biosphere net sink derived from $\delta^{13}\text{C}$ during the 1990s [*Battle et al.*, 2000], O_2/N_2 levels may also respond to the large perturbations in ocean NPP and circulation that occurred during the decade. In the *Battle et al.* [2000] inversion of carbon sources and sinks, retrieval of land and ocean sinks with O_2/N_2 assumed that all changes in O_2/N_2 originated from the terrestrial biosphere and fossil fuels; ocean contributions were assumed to be invariant. Given the large changes in ocean circulation and biogeochemistry that occurred during the 1997/1998 El Niño, it is possible that oceans contributed to some of the atmospheric O_2/N_2 variability. For example, *Behrenfeld et al.* [2001] found that

ocean NPP increased by 5 Pg C/yr from 1997 to 2000, during an El Niño/La Niña transition, primarily in the eastern tropical Pacific.

4.4. Next Steps

[51] We designed our double deconvolution analysis to demonstrate the consequences of time-varying terrestrial C3 discrimination for the global atmospheric carbon budget. It was not meant to be a comprehensive treatment of $\delta^{13}\text{C}$ and CO_2 . We ignored several crucial processes. Specifically, shifts in C3 and C4 plant may also induce disequilibria [*Ciais et al.*, 1999; *Townsend et al.*, 2002; *Still et al.*, 2002]. These shifts must be treated in the same way C3 fluxes are considered here, in terms of the isotopic forcing of gross photosynthesis and the gross biosphere-atmosphere return flux (mostly respiration, volatile organic carbon emissions, and fires). Interannual changes of a percent or two in the relative contribution of C3 and C4 GPP would have a comparable effect to the anomalies in C3 discrimination described here, and could either amplify or cancel variability in C3 discrimination caused by drought associated with ENSO. Indeed, many of the large drought stress anomalies associated with ENSO (Figure 2c) are in areas with predominantly C3 vegetation. A decline in total C3 GPP relative to C4 GPP would have a similar impact on the global atmospheric ^{13}C budget as the drought in C3 ecosystems described here.

[52] In addition, we neglected variation in ocean disequilibria: by using a single average value from the work of *Gruber et al.* [1999]. As the ocean to atmosphere ^{13}C flux depends strongly on the $\delta^{13}\text{C}$ of pCO_2 in ocean surface layers [*Gruber et al.*, 1999; *Zhang et al.*, 1995], it will vary with changes in ocean biology [*Behrenfeld et al.*, 2001], sea surface temperature [*Reynolds and Smith*, 1994], and salinity that accompany El Niño events.

5. Conclusions

[53] Small changes in terrestrial discrimination have significant impacts on regional and global ^{13}C budgets. While this complicates the direct use of $\delta^{13}\text{C}$ and CO_2 for land ocean partitioning, recent success in characterizing discrimination responses to climate at the ecosystem scale suggest that these responses are predictable, and in the future it will be possible to characterize and isolate their contribution. Three primary points of the paper are summarized below:

1. The terrestrial biosphere, as a whole, undergoes drought stress during major El Niño events.
2. Field observations, tree ring analyses, and eco-physiological models suggest that for many C3 ecosystems, GPP and discrimination simultaneously decrease in response to drought stress.
3. Relatively small changes in global ^{13}C discrimination (<1‰) can have a significant impact on atmospheric ^{13}C content because they are associated with the one-way GPP flux. Equations describing isotopic exchange with the terrestrial biosphere need to allow for this possibility. If discrimination and the net land sink covary in response to El Niño (consistent with a decrease in C3 GPP), then less interannual variability in land and ocean sinks is required to simultaneously reconcile ^{13}C and CO_2 atmospheric budgets

as compared with past applications of the double deconvolution approach that have assumed a constant discrimination.

Appendix A

[54] Considering only the terrestrial biosphere, ¹³C fluxes can be represented in δ notation as the sum of the isotopic forcing from the one-way fluxes of GPP and R_b .

$$\frac{d(\delta_a C_a)}{dt} \cong G_b(\delta_a - \Delta_{ab}) + R_b \delta_{ba} \quad (\text{A1})$$

where Δ_{ab} can be represented as the sum of an anomaly component, $\dot{\Delta}_{ab}$, and a mean, $\bar{\Delta}_{ab}$:

$$\frac{d(\delta_a C_a)}{dt} \cong G_b(\delta_a - \bar{\Delta}_{ab} - \dot{\Delta}_{ab}) + R_b \delta_{ba} \quad (\text{A2})$$

Assuming that $G_b \dot{\Delta}_{ab}$ is equal to zero (that discrimination is invariant), A2 simplifies to:

$$\frac{d(\delta_a C_a)}{dt} \cong -G_b \bar{\Delta}_{ab} + G_b \delta_a + R_b \delta_{ba} \quad (\text{A3})$$

[55] Now, let the net land carbon sink, N_b , equal the sum of GPP (G_b) and the biosphere-atmosphere return flux (R_b):

$$N_b = G_b + R_b \quad (\text{A4})$$

Also, if plant discrimination is constant, then the isotopic composition of ecosystem respiration (δ_{ba}) in equation A3 is given by:

$$\delta_{ba} = \delta_a - \bar{\Delta}_{ab} + (\delta_a^e - \delta_a) \quad (\text{A5})$$

where $\delta_a^e - \delta_a$ is known as the isotopic disequilibrium, and is equal to the difference between the contemporary atmosphere, δ_a , and a past atmosphere, δ_a^e , that represents the composition of the atmosphere when R_b was fixed.

[56] Substituting equations A4 and A5 into A3, we obtain the conventional double deconvolution representation of the terrestrial biosphere:

$$\frac{d(\delta_a C_a)}{dt} \cong N_b(\delta_a - \bar{\Delta}_{ab}) + R_b(\delta_a^e - \delta_a) \quad (\text{A6})$$

[57] **Acknowledgments.** This work was supported by a NASA MDAR grant to Randerson (NAG5-9462) and to Fung (NAG5-11200). We wish to thank J. Adkins and C. Field for helpful discussions.

References

Aerts, R., and F. S. Chapin, The mineral nutrition of wild plants revisited: A re-evaluation of processes and patterns, *Adv. Ecol. Res.*, 30, 1–67, 2000.
 Andres, R. J., G. Marland, T. Boden, and S. Bischof, Carbon dioxide emissions from fossil fuel consumption and cement manufacture, 1751–1991, and an estimate of their isotopic composition and latitudinal distribution, in *The Carbon Cycle*, edited by T. M. L. Wigley and D. S. Schimel, pp. 53–62, Cambridge Univ. Press, New York, 2000.
 Ares, A., and J. H. Fownes, Water supply regulates structure, productivity, and water use efficiency of *Acacia koa* forest in Hawaii, *Oecologia*, 121, 458–466, 1999.

Asner, G. P., A. R. Townsend, and B. H. Braswell, Satellite observation of El Niño effects on Amazon forest phenology and productivity, *Geophys. Res. Lett.*, 27(7), 981–984, 2000.
 Barber, V., G. Juday, and B. Finney, Reduced growth of Alaskan white spruce in the twentieth century from temperature-induced drought stress, *Nature*, 405, 668–673, 2000.
 Battle, M., M. L. Bender, P. P. Tans, J. W. C. White, J. T. Ellis, T. Conway, and R. J. Francey, Global carbon sinks and their variability inferred from atmospheric O₂ and $\delta^{13}\text{C}$, *Science*, 287, 2467–2470, 2000.
 Behrenfeld, M. J., et al., Biospheric primary production during an ENSO transition, *Science*, 291, 2594–2597, 2001.
 Berry, J. A., Studies of mechanisms affecting the fractionation of carbon isotopes in photosynthesis, in *Stable Isotopes in Ecological Research*, edited by J. R. Ehleringer, K. A. Nagy, and P. W. Rundel, pp. 84–88, Springer-Verlag, New York, 1987.
 Bishop, J. K. B., and W. B. Rossow, Spatial and temporal variability of global surface solar irradiance, *J. Geophys. Res.*, 96, 16,839–16,858, 1991.
 Bowling, D. R., N. G. McDowell, B. J. Bond, B. E. Law, and J. R. Ehleringer, C-13 content of ecosystem respiration is linked to precipitation and vapor pressure deficit, *Oecologia*, 131, 113–124, 2002.
 Braswell, B. H., D. S. Schimel, E. Linder, and B. I. Moore, The response of global terrestrial ecosystems to interannual temperature variability, *Science*, 278, 870–872, 1997.
 Ciais, P., P. P. Tans, J. W. C. White, M. Trolier, R. J. Francey, J. A. Berry, D. A. Randall, P. J. Sellar, J. G. Collatz, and D. S. Schimel, Partitioning ocean and land uptake of CO₂ as inferred by $\delta^{13}\text{C}$ measurements from the NOAA Climate Monitoring and Diagnostics Laboratory global air sampling network, *J. Geophys. Res.*, 100, 5051–5070, 1995.
 Ciais, P., P. Friedlingstein, D. S. Schimel, and P. P. Tans, A global calculation of the delta C-13 of soil respired carbon: Implications for the biospheric uptake of anthropogenic CO₂, *Global Biogeochem. Cycles*, 13(2), 519–530, 1999.
 Conway, T. J., P. P. Tans, P. M. Lang, K. A. Masarie, K. Thoning, N. Paynter, D. Kitzis, J. W. C. White, and V. B., Recent variations in the atmospheric CO₂ growth rate, paper presented at 2001 Annual Meeting, NOAA Clim. Monit. and Diagnostics Lab., Boulder, Colo., 2001.
 Crutzen, P. J., and M. O. Andreae, Biomass burning in the tropics: Impacts on atmospheric chemistry and biogeochemical cycles, *Science*, 250, 1669–1678, 1990.
 Dai, A., I. Y. Fung, and A. D. Del Genio, Surface observed global land precipitation variations during 1900–88, *J. Clim.*, 10, 2943–2962, 1997.
 Dai, A., K. E. Trenberth, and T. R. Karl, Global variations in droughts and wet spells: 1900–1995, *Geophys. Res. Lett.*, 25(17), 3367–3370, 1998.
 DeFries, R. S., and J. R. G. Townshend, NDVI-derived land cover classifications at a global scale, *Int. J. Remote Sens.*, 15(17), 3567–3586, 1994.
 DeFries, R. S., M. C. Hansen, J. R. G. Townshend, A. C. Janetos, and T. R. Loveland, A new global 1-km dataset of percentage tree cover derived from remote sensing, *Global Change Biol.*, 6(2), 247–254, 2000.
 Ehleringer, J., Carbon and water relations in desert plants: An isotopic perspective, in *Stable Isotopes and Plant Carbon-Water Relations*, pp. 155–172, Academic, San Diego, Calif., 1993.
 Ekblad, A., and P. Hogberg, Natural abundance of C-13 in CO₂ respired from forest soils reveals speed of link between tree photosynthesis and root respiration, *Oecologia*, 127, 305–308, 2001.
 Emanuel, W. R., G. E. G. Killough, and J. S. Olson, Modelling the circulation of carbon in the world's terrestrial ecosystems, in *Carbon Cycling Modelling*, edited by B. Bolin, pp. 335–353, John Wiley, New York, 1981.
 Enting, I. G., C. M. Trudinger, R. J. Francey, and H. Granek, Synthesis inversion of atmospheric CO₂ using the GISS tracer transport model, *Tech. Pap. 29*, CSIRO Div. of Atmos. Res., Canberra, Australia, 1993.
 Enting, I. G., C. M. Trudinger, and R. J. Francey, A synthesis inversion of the concentration and $\delta^{13}\text{C}$ of atmospheric CO₂, *Tellus, Ser. B*, 47, 35–52, 1995.
 Evans, J. R., and F. Loreto, Acquisition and diffusion of CO₂ in higher plant leaves, in *Photosynthesis: Physiology and Metabolism*, edited by R. C. Leegood, T. D. Sharkey, and S. von Caemmerer, pp. 321–351, Kluwer Acad., Norwell, Mass., 2000.
 Farquhar, G. D., M. H. O'Leary, and J. A. Berry, On the relationship between carbon isotope discrimination and the intercellular carbon dioxide concentration in leaves, *Austral. J. Plant Physiol.*, 9, 121–137, 1982.
 Farquhar, G. D., J. R. Ehleringer, and K. T. Hubick, Carbon isotope discrimination and photosynthesis, *Annu. Rev. Plant Physiol. Plant Mol. Biol.*, 40, 503–537, 1989.

- Feely, R. A., R. Wanninkhof, C. Goyet, D. E. Archer, and T. Takahashi, Variability of CO₂ distributions and sea-air fluxes in the central and eastern equatorial Pacific during the 1991–1994 El Niño, *Deep Sea Res., Part II*, 44(9–10), 1851–1867, 1997.
- Feely, R. A., R. Wanninkhof, T. Takahashi, and P. Tans, Influence of El Niño on the equatorial Pacific contribution to atmospheric CO₂ accumulation, *Nature*, 398, 597–601, 1999.
- Flanagan, L. B., J. R. Brooks, and J. R. Ehleringer, Photosynthesis and carbon isotope discrimination in boreal forest ecosystems: A comparison of functional characteristics in plants from three mature forest types, *J. Geophys. Res.*, 102, 28,861–28,869, 1997.
- Francey, R. J., P. P. Tans, C. E. Allison, I. G. Enting, J. W. C. White, and M. Trolter, Changes in oceanic and terrestrial carbon uptake since 1982, *Nature*, 373, 326–330, 1995.
- Francey, R. J., C. E. Allison, D. M. Etheridge, C. M. Trudinger, I. G. Enting, M. Leuenberger, R. L. Langenfelds, E. Michel, and L. P. Steele, A 1000-year high precision record of delta C-13 in atmospheric CO₂, *Tellus, Ser. B*, 51, 170–193, 1999.
- Fung, I. Y., et al., Carbon 13 exchanges between the atmosphere and biosphere, *Global Biogeochem. Cycles*, 11(4), 507–533, 1997.
- Gaudinski, J. B., S. E. Trumbore, E. A. Davidson, and S. H. Zheng, Soil carbon cycling in a temperate forest: Radiocarbon-based estimates of residence times, sequestration rates and partitioning of fluxes, *Biogeochemistry*, 51(1), 33–69, 2000.
- Gerard, J. C., B. Nemry, L. M. Francois, and P. Warnant, The interannual change of atmospheric CO₂: Contribution of subtropical ecosystems?, *Geophys. Res. Lett.*, 26(2), 243–246, 1999.
- Goldstein, A. H., N. E. Hultman, J. M. Fracheboud, M. R. Bauer, J. A. Panek, M. Xu, Y. Qi, A. B. Guenther, and W. Baugh, Effects of climate variability on the carbon dioxide, water, and sensible heat fluxes above a ponderosa pine plantation in the Sierra Nevada (CA), *Agric. For. Meteorol.*, 101(2–3), 113–129, 2000.
- Goulden, M. L., J. W. Munger, S. M. Fan, B. C. Daube, and S. C. Wofsy, Exchange of carbon dioxide by a deciduous forest: Response to inter-annual climate variability, *Science*, 271, 1576–1578, 1996.
- Gruber, N., and C. D. Keeling, An improved estimate of the isotopic air-sea disequilibrium of CO₂: Implications for the oceanic uptake of anthropogenic CO₂, *Geophys. Res. Lett.*, 28(3), 555–558, 2000.
- Gruber, N., C. D. Keeling, R. B. Bacastow, P. R. Guenther, T. J. Lueker, M. Wahlen, H. A. J. Meijer, W. G. Mook, and T. F. Stocker, Spatiotemporal patterns of carbon-13 in the global surface oceans and the oceanic Suess effect, *Global Biogeochem. Cycles*, 13(2), 307–335, 1999.
- Hansen, J., and S. Lebedeff, Global trends of surface air temperature, *J. Geophys. Res.*, 92, 13,345–13,372, 1987.
- Hansen, J., R. Ruedy, J. Glascoe, and M. Sato, GISS analysis of surface temperature change, *J. Geophys. Res.*, 104, 30,997–31,022, 1999.
- Huffman, G. J., R. F. Adler, P. Arkin, A. Chang, R. Ferraro, A. Gruber, J. Janowiak, A. McNab, B. Rudolf, and U. Schneider, The Global Precipitation Climatology Project (GPCP) combined precipitation dataset, *Bull. Am. Meteorol. Soc.*, 78(1), 5–20, 1997.
- Janicot, S., V. Moron, and B. Fontaine, Sahel droughts and ENSO dynamics, *Geophys. Res. Lett.*, 23(5), 515–518, 1996.
- Joos, F., and M. Bruno, Long-term variability of the terrestrial and oceanic carbon sinks and the budgets of the carbon isotopes ¹³C and ¹⁴C, *Global Biogeochem. Cycles*, 12(12), 277–296, 1998.
- Keeling, C. D., T. P. Whorf, M. Wahlen, and J. van der Plicht, Interannual extremes in the rate of rise of atmospheric carbon dioxide since 1980, *Nature*, 375, 666–669, 1995.
- Keeling, R. F., S. C. Piper, and M. Heimann, Global and hemispheric sinks deduced from changes in atmospheric O₂ concentrations, *Nature*, 381, 218–221, 1996.
- Kistler, R., et al., The NCEP-NCAR 50-year reanalysis: Monthly means CD-ROM and documentation, *Bull. Am. Meteorol. Soc.*, 82(2), 247–267, 2001.
- Kogan, F. N., Satellite-observed sensitivity of world land ecosystems to El Niño/La Niña, *Remote Sens. Environ.*, 74(3), 445–462, 2000.
- Kripalani, R. H., and A. Kulkarni, Rainfall variability over South-east Asia—Connections with Indian monsoon and ENSO extremes: New perspectives, *Int. J. Climatol.*, 17(11), 1155–1168, 1997.
- Lee, K., R. Wanninkhof, T. Takahashi, S. C. Doney, and R. A. Feely, Low interannual variability in recent oceanic uptake of atmospheric carbon dioxide, *Nature*, 396, 155–159, 1998.
- Livingston, N. J., and D. L. Spittlehouse, Carbon isotope fractionation in tree rings in relation to the growing season water balance, in *Stable Isotopes and Plant Carbon-Water Relations*, edited by J. R. Ehleringer, A. E. Hall, and G. D. Farquhar, pp. 141–154, Academic, San Diego, Calif., 1993.
- Lloyd, J., and G. D. Farquhar, ¹³C discrimination during CO₂ assimilation by the terrestrial biosphere, *Oecologia*, 99, 201–215, 1994.
- Lloyd, J., and J. A. Taylor, On the temperature dependence of soil respiration, *Funct. Ecol.*, 8, 315–323, 1994.
- Los, S. O., C. O. Justice, and C. J. Tucker, A global 1x1 NDVI data set for climate studies derived from GIMMS continental NDVI data, *Int. J. Remote Sens.*, 15(17), 3493–3518, 1994.
- Los, S. O., G. J. Collatz, L. Bounoua, P. J. Sellers, and C. J. Tucker, Global interannual variations in sea surface temperature and land surface vegetation, air temperature, and precipitation, *J. Clim.*, 14, 1535–1549, 2001.
- Maisongrande, P., A. Ruimy, G. Dedieu, and B. Saugier, Monitoring seasonal and interannual variations of gross primary productivity, net primary productivity and net ecosystem productivity using a diagnostic model and remotely-sensed data, *Tellus, Ser. B*, 47(1–2), 178–190, 1995.
- Matsueda, H., and H. Y. Inoue, Aircraft measurements of trace gases between Japan and Singapore in October of 1993, 1996, and 1997, *Geophys. Res. Lett.*, 26(16), 2413–2416, 1999.
- McNulty, S. G., and W. T. Swank, Wood δ¹³C as a measure of annual basal area growth and soil-water stress in a pinus-strobus forest, *Ecology*, 76(5), 1581–1586, 1995.
- Neff, J. C., and G. P. Asner, Dissolved organic carbon in terrestrial ecosystems: Synthesis and a model, *Ecosystems*, 4(1), 29–48, 2001.
- Nepstad, D. C., C. R. Carva, E. A. Davidson, P. H. Jipp, P. A. Lefebvre, G. H. Negreiros, E. D. da Silva, T. A. Stone, S. E. Trumbore, and S. Vieira, The role of deep roots in hydrological and carbon of Amazonian forests and pastures, *Nature*, 372, 666–669, 1994.
- Nepstad, D. C., et al., Large-scale impoverishment of Amazonian forests by logging and fire, *Nature*, 398, 505–508, 1999.
- Pate, J., and D. Arthur, delta C-13 analysis of phloem sap carbon: Novel means of evaluating seasonal water stress and interpreting carbon isotope signatures of foliage and trunk wood of Eucalyptus globulus, *Oecologia*, 117, 301–311, 1998.
- Potter, C. S., and S. A. Klooster, Detecting a terrestrial biosphere sink for carbon dioxide: Interannual ecosystem modeling for the mid-1980s, *Clim. Change*, 42(3), 489–503, 1999.
- Raich, J. W., and C. S. Potter, Global patterns of carbon dioxide emissions from soils, *Global Biogeochem. Cycles*, 9(1), 23–36, 1995.
- Randerson, J. T., M. V. Thompson, T. J. Conway, I. Y. Fung, and C. B. Field, The contribution of terrestrial sources and sinks to trends in the seasonal cycle of atmospheric carbon dioxide, *Global Biogeochem. Cycles*, 11(4), 535–560, 1997.
- Reynolds, R. W., and T. M. Smith, Improved global sea-surface temperature analyses using optimum interpolation, *J. Clim.*, 7, 929–948, 1994.
- Ropelewski, C. F., and M. S. Halpert, Quantifying Southern Oscillation-precipitation relationships, *J. Clim.*, 9, 1043–1059, 1996.
- Ryan, M. G., Effects of climate change on plant respiration, *Ecol. Appl.*, 1(2), 157–167, 1991.
- Saurer, M., U. Siegenthaler, and F. Schweingruber, The climate-carbon isotope relationship in tree-rings and the significance of site conditions, *Tellus, Ser. B*, 47(3), 320–330, 1995.
- Schuur, E. A. G., M. C. Mack, J. W. Harden, and S. E. Trumbore, Isotopic composition of carbon dioxide from a boreal forest fire: Inferring carbon loss from measurements and modeling, *Global Biogeochem. Cycles*, 16, doi:10.1029/2001GB001840, in press, 2002.
- Sellers, P. J., W. J. Shuttleworth, J. L. Dorman, A. Dalcher, and J. M. Roberts, Calibrating the Simple Biosphere Model for Amazonian tropical forest using field and remote-sensing data, 1, Average calibration with field data, *J. Appl. Meteorol.*, 28(8), 727–759, 1989.
- Sellers, P. J., S. O. Los, C. J. Tucker, C. O. Justice, D. A. Dazlich, G. J. Collatz, and D. A. Randall, A revised land surface parameterization (SiB2) for atmospheric GCMs, 2, The generation of global fields of terrestrial biophysical parameters from satellite data, *J. Clim.*, 9, 706–737, 1996a.
- Sellers, P. J., D. A. Randall, G. J. Collatz, J. A. Berry, C. B. Field, D. A. Dazlich, C. Zhang, G. D. Collalo, and L. Bounoua, A revised land-surface parameterization (SiB2) for atmospheric GCMs, 1 Model formulation, *J. Clim.*, 9, 676–705, 1996b.
- Still, C. J., J. A. Berry, G. J. Collatz, and R. S. DeFries, The global distribution of C3 and C4 vegetation: Carbon cycle implications, *Global Biogeochem. Cycles*, 16, doi:10.1029/2001GB01807, in press, 2002.
- Stuiver, M., R. L. Burk, and P. D. Quay, ¹³C/¹²C ratios in tree rings and the transfer of biospheric carbon to the atmosphere, *J. Geophys. Res.*, 89, 11,731–11,748, 1984.
- Susskind, J., P. Piraino, L. Rokke, T. Iredell, and A. Mehta, Characteristics of the TOVS Pathfinder Path A dataset, *Bull. Am. Meteorol. Soc.*, 78(7), 1449–1472, 1997.
- Tans, P. P., J. A. Berry, and R. F. Keeling, Oceanic ¹³C/¹²C observations: A new window on ocean CO₂ uptake, *Global Biogeochem. Cycles*, 7(2), 353–368, 1993.

- Thompson, M. V., and J. T. Randerson, Impulse response functions of terrestrial carbon cycle models: Method and application, *Global Change Biol.*, 5, 371–394, 1999.
- Thompson, M. V., J. T. Randerson, C. M. Malmstrom, and C. B. Field, Change in net primary production and heterotrophic respiration: How much is necessary to sustain the terrestrial carbon sink?, *Global Biogeochem. Cycles*, 10(4), 711–726, 1996.
- Tian, H. Q., J. M. Melillo, D. W. Kicklighter, A. D. McGuire, J. V. K. Helfrich, B. Moore, and C. J. Vorosmarty, Effect of interannual climate variability on carbon storage in Amazonian ecosystems, *Nature*, 396, 664–667, 1998.
- Townsend, A. R., G. P. Asner, J. W. C. White, and P. P. Tans, Land use effects on atmospheric ¹³C imply a sizable terrestrial CO₂ sink in tropical latitudes, *Geophys. Res. Lett.*, 29(10), 1426, 10.1029/2001GL013454, 2002.
- Trudinger, C. M., I. G. Enting, R. J. Francey, D. M. Etheridge, and P. J. Rayner, Long-term variability in the global carbon cycle inferred from a high-precision CO₂ and ¹³C ice-core record, *Tellus, Ser. B*, 51(2), 233–248, 1999.
- Villalba, R., and T. T. Veblen, Influences of large-scale climatic variability on episodic tree mortality in northern Patagonia, *Ecology*, 79(8), 2624–2640, 1998.
- Winguth, A. M. E., M. Heimann, K. D. Kurz, E. Maierreimer, U. Mikolajewicz, and J. Segschneider, El-Niño-Southern Oscillation related fluctuations of the marine carbon-cycle, *Global Biogeochem. Cycles*, 8(1), 39–63, 1994.
- Wong, S. C., I. R. Cowan, and G. D. Farquhar, Stomatal conductance correlates with photosynthetic capacity, *Nature*, 282, 424–426, 1979.
- Woodwell, G. M., and R. H. Whittaker, Primary production in terrestrial ecosystems, *Am. Zool.*, 8, 19–30, 1968.
- Wullschleger, S. D., W. M. Post, and A. W. King, On the potential for a CO₂ fertilization effect in forests: Estimates of the biotic growth factor based on 58 controlled-exposure studies, in *Biotic Feedbacks in the Global Climate System: Will the Warming Feed the Warming?*, edited by G. M. Woodwell and F. T. MacKenzie, pp. 85–107, Oxford Univ. Press, New York, 1995.
- Yang, X., and M. Wang, Monsoon ecosystems control on atmospheric CO₂ interannual variability: Inferred from a significant positive correlation between year-to-year changes in land precipitation and atmospheric CO₂ growth rate, *Geophys. Res. Lett.*, 27(11), 1671–1674, 2000.
- Zhang, J., P. D. Quay, and D. O. Wilbur, Carbon-isotope fractionation during gas-water exchange and dissolution of CO₂, *Geochim. Cosmochim. Acta*, 59(1), 107–114, 1995.
- Zhang, J. W., Z. Feng, B. M. Cregg, and C. M. Schumann, Carbon isotopic composition, gas exchange, and growth of three populations of ponderosa pine differing in drought tolerance, *Tree Physiol.*, 17(7), 461–466, 1997.
- J. A. Berry, Carnegie Institution of Washington, Department of Plant Biology, 260 Panama St., Stanford, CA 94305-1297, USA. (joeberry@catalase.stanford.edu)
- G. J. Collatz, Goddard Space Flight Center, Code 923, Greenbelt, MD 20771, USA. (jcollatz@biome.gsfc.nasa.gov)
- A. S. Denning and N. Suits, Department of Atmospheric Sciences, Colorado State University, Fort Collins, CO 80523, USA. (denning@atmos.colostate.edu; nsuits@atmos.colostate.edu)
- J. E. Fessenden, Hydrology, Geochemistry and Geology Group, Earth and Environmental Sciences Division, Los Alamos National Laboratory, EES-6, MS-D462, Los Alamos, NM 87545, USA. (julianna@lanl.gov)
- I. Y. Fung and C. J. Still, Center for Atmospheric Sciences, University of California Berkeley, 4767 McCone Hall, Berkeley, CA 94720-4767, USA. (inez@sequoia.atmos.berkeley.edu; still@sequoia.atmos.berkeley.edu)
- A. D. Munoz and J. T. Randerson, Divisions of Geological and Planetary Sciences and Engineering and Applied Science, California Institute of Technology, Mail Stop 100-23, Pasadena, CA 91125, USA. (munoz@its.caltech.edu; jimr@gps.caltech.edu)